WP15ER-CPR(17) 18174

M Hoelzl et al.

What non-linear simulations can teach about ELM physics

Preprint of Paper to be submitted for publication in Proceeding of 16th International Workshop on Plasma Edge Theory in Fusion Devices (PET)

This work has been carried out within the framework of the EUROfusion Consortium and has received funding from the Euratom research and training programme 2014-2018 under grant agreement No 633053. The views and opinions expressed herein do not necessarily reflect those of the European Commission.

Article Type????

Insights into type-I ELMs and ELM control methods from JOREK non-linear MHD simulations

M. Hoelzl*,[1] G.T.A. Huijsmans,[2,3] F. Orain,[1] F.J. Artola,[4] S. Pamela,[5] M. Becoulet,[2] D. van Vugt,[3] F. Liu,[2,6] S. Futatani,[7] A. Lessig,[1] E. Wolfrum,[1] F. Mink,[1] E. Trier,[1] M. Dunne,[1] E. Viezzer,[1] T. Eich,[1] B. Vanovac,[8] L. Frassinetti,[9] S. Guenter,[1] K. Lackner,[1] I. Krebs,[10] ASDEX Upgrade Team,[1] and EUROfusion MST1 Team[11]

[1] *Max-Planck-Institute for Plasma Physics, Boltzmannstr. 2, 85748 Garching b. M., Germany*
[2] *CEA, IRFM, 13108 Saint-Paul-Lez-Durance, France*
[3] *Eindhoven University of Technology, P.O. Box 513, 5600 MB Eindhoven, The Netherlands*
[4] *Aix-Marseille University, CNRS, PIIM UMR 7345, 13397 Marseille Cedex 20, France*
[5] *CCFE, Culham Science Centre, OX14 3DB, UK*
[6] *Université Côte d'Azur, Laboratoire J.A. Dieudonné UMR nř 7351 CNRS UNS 06108 Nice Cedex 02, France*
[7] *Barcelona Supercomputing Center, Barcelona, Spain*
[8] *DIFFER, Dutch Institute for Fundamental Energy research, The Netherlands*
[9] *Division of Fusion Plasma Physics, KTH Royal Institute of Technology, Stockholm, SE, Sweden*
[10] *Princeton Plasma Physics Laboratory, P.O. Box 451, Princeton NJ 08543, USA*
[11] *See author list of [H. Meyer et al 2017 Nucl. Fusion 57 102014]*

Correspondence: *Email: matthias.hoelzl@ipp.mpg.de

Present Address: xxx

Received xxx; Revised xxx; Accepted xxx

Summary

Edge localized modes (ELMs) are repetitive instabilities driven by the large pressure gradients and current densities in the edge of H-mode plasmas. Type-I ELMs lead to a fast collapse of the H-mode pedestal within several hundred μs to few ms. Localized transient heat fluxes to divertor targets are expected to exceed tolerable limits for ITER requiring advanced insights into ELM physics and applicable mitigation methods. This article describes how non-linear MHD simulations contribute to the research. The JOREK code is introduced which allows to study large-scale plasma instabilities in tokamak X-point plasmas covering main plasma, scrape off layer and divertor region with its finite element grid.

We review key physics processes relevant for type-I ELMs and show to which extent JOREK simulations agree with experiments and help reveal underlying mechanisms. Simulations and experimental findings are compared in many respects for type-I ELMs in ASDEX Upgrade. The role of plasma flows and non-linear mode coupling for the spatial and temporal structure of ELMs are emphasized and loss mechanisms are discussed. An overview of recent ELM related research using JOREK is given including ELM crashes, ELM free regimes, ELM pacing by pellets and magnetic kicks, and mitigation or suppression by resonant magnetic perturbation coils (RMPs). Simulations of ELMs and ELM control methods agree in many respects with experimental observations from various tokamak experiments. On this basis, predictive simulations become

more and more feasible. A brief outlook is given showing main priorities for further research in the field of ELM physics and further developments necessary.

Keywords: tokamak, MHD, ELMs, ballooning mode, mode coupling, stochastic field, ELM control, JOREK

1 Introduction

When the high-confinement mode (H-mode) was discovered in 1982 in the ASDEX divertor tokamak, the authors also reported about "short bursts [...] which lead to periodic density and temperature reductions in the outer plasma zone"[81]. For these bursts, the name "edge localized modes (ELMs)" was introduced[36] and different classes of ELMs were identified as summarized e.g. in Refs.[9, 87]. Type-I ELMs are the largest and most common edge instability in H-mode plasmas associated with losses of typically up to 10% of the total plasma thermal energy and particles on a time scale of several hundred μs to few ms. For ITER, regression analysis predicts relative ELM sizes larger than in present machines and divertor heat fluxes exceeding the limits acceptable for a reasonably long material lifetime[44]. Consequently, research on natural ELM-free regimes like Quiescent H-Mode (QH-Mode)[5, 23], ELM pacing via pellet injection[41] or magnetic kicks[7], and ELM mitigation respectively suppression via resonant magnetic perturbation fields (RMPs)[14] has moved into the focus of research aiming to reduce divertor heat loads.

Linear MHD analysis of the plasma stability has identified ideal ballooning modes as the main instability responsible for type-I ELM crashes (e.g., Refs. [22, 69]). However, only non-linear simulations allow to investigate the underlying non-linear physics processes of ELMs and the relevant control methods. A comprehensive review of non-linear simulations of ELMs and their control by various codes can be found in Reference[32].

The non-linear MHD code JOREK is described in Section 2. Section 3 reviews key physics mechanisms relevant for ELM crashes, shows to which extent simulations agree with experiments and how they promote a basic understanding of ELM physics. On the example of ASDEX Upgrade[73], it is demonstrated that quantitative agreement is obtained between simulations and experiments in many respects. At the same time, a brief overview is given of recent ELM related simulations performed with JOREK. Recent advances demonstrate that simulations are undergoing a transition from a qualitative description of ELM physics and ongoing validation towards predictive capabilities. An overview of ELM control methods is given in Section 4: ELM free regimes, ELM pacing via pellet injection and magnetic kicks, as well as mitigation and suppression by RMPs. For each control method, the principles are briefly explained and an overview of results from JOREK is given. Conclusions and an outlook are provided in Section 5.

2 The JOREK code

The non-linear MHD code JOREK[35] allows to investigate large-scale instabilities in divertor tokamaks. It applies a C^1 continuous flux surface aligned 2D Bezier mesh[6] and a toroidal Fourier representation to discretize plasma, scrape-off layer, and divertor. Ideal wall boundary conditions and sheath boundary conditions at geometrically simplified divertor targets apply. The initial fields produced by a built-in Grad-Shafranov solver are advanced in time fully implicitly allowing to use time steps independent of grid resolution. The sparse matrix system is solved with an iterative GMRES scheme preconditioned by solving matrix blocks corresponding to individual toroidal harmonics using the direct sparse matrix solver PaStiX[25] (which is the limiting factor in terms of memory consumption and parallel scalability). A hybrid OpenMP/MPI approach is used for parallelization where typically one or few MPI tasks are used per compute node. Collaborative code development is performed via a git shared repository with automatic tests, code reviewing, and a documentation Wiki.

Results presented in this article are based on a reduced MHD physics model including neoclassical and diamagnetic effects[54] which fulfills energy conservation properties[18]. Full MHD equations are available[24] and presently being extended by two-fluid effects, sheath boundary conditions, and stabilization methods. A free boundary extension for coils and resistive walls replacing ideal wall conditions is realized via a coupling[27] to STARWALL[48]. A pellet ablation model[21], a full-orbit particle tracer including ionization, recombination and background collisions[76], a neutrals model[15], and a relativistic electron guiding center particle tracer[70] are available. An impurity model[53] and a relativistic electron fluid model are presently being validated.

JOREK is broadly applied to large-scale plasma instabilities in tokamak plasmas. ELM related activities are the subject of this article. Disruption-related research includes (neoclassical) tearing modes[49] and their control[62], thermal and current quench including massive gas injection[15, 53] and shattered pellet injection[31], vertical displacement events[30] as well as runaway electrons[70].

3 Type-I ELMs

This section reviews key physics mechanisms of type-I ELMs. Results from ASDEX Upgrade ELM simulations are shown and compared to key features of experiments giving some insight into basic mechanisms. An overview of recent research on ELM physics with JOREK is given as well.

3.1 Setup for the ASDEX Upgrade ELM simulations

The simulations shown in the following are based on a typical ASDEX Upgrade H-mode equilibrium with an edge safety factor of $q_{95} = 5.9$. The experimentally observed type-I ELM crashes take about 2ms corresponding to so-called long ELMs[19, 20, 67]. A pre-ELM equilibrium reconstruction (ASDEX Upgrade discharge #33616 at 7.2s) performed by the CLISTE code[47] is used for initial conditions which is already unstable such that the simulations only allow to investigate the ELM crash itself, but not the inter-ELM phase. The plasma resistivity is increased from the Spitzer value by a factor of eight for computational reasons. The parallel heat diffusivity is taken to be two orders of magnitude smaller than Spitzer-Härm predictions[71] to account for the heat-flux limit[26, 46]. Neoclassical and diamagnetic flows are taken into account. Toroidal harmonics $n = 0 \dots 8$ are included in the main simulations. Additional tests have been done to verify that mode numbers beyond $n = 8$ are subdominant. Linearly we have tested mode numbers up to 24 showing that high mode numbers are subdominant due to the stabilizing effects of ExB and diamagnetic flows. As a non-linear test we have restarted our simulations with $n = 0 \dots 13$ instead of $n = 0 \dots 8$ for about 0.2 ms during the ELM crash. The $n = 9 \dots 13$ harmonics remain by about one order of magnitude smaller than the $n = 3, 4$ modes dominant in this phase. Running the whole simulation with more harmonics would be possible with the present code, but computationally expensive. We would make use of that for cases where this is really necessary. In parallel numerical work on the solver is performed in order to reduce the computational effort for large toroidal resolutions.

3.2 Inter-ELM phase

After an ELM crash, pedestal pressure gradients are moderate. Consequently edge current densities are low which are dominated by the bootstrap current[65]. Also the $E \times B$ rotation is strongly reduced since it is in the pedestal region described by neoclassical physics[79]. Due to the H-mode transport barrier, the density and temperature pedestals start to build up[86]. In experiments, the maximum pressure gradient in many cases increases up to a certain value and remains there for several ms before an ELM crash occurs[4]. The EPED model[68] predicts, that when a critical pressure gradient for kinetic ballooning modes is reached, these modes lead to a clamping of the pressure gradient. A correlation of this clamping with high frequency modes has been confirmed experimentally[8, 38] although Laggner et al could not confirm the ballooning character of the observed modes. Typically, while the maximum pressure gradient remains clamped, the pedestal is growing further inwards until a large ELM crash appears. Often, precursor modes are observed before which have a similar spatial structure as the ELM crash[17, 61]. JOREK simulations so far did not concentrate strongly on the inter-ELM phase. Multiple ELM cycles have been obtained[2, 55], with artificially increased sources such that repetition frequencies are higher than for type-I ELMs. Refined simulations will investigate realistic type-I ELM cycles and give a deeper insight into inter-ELM phase and ELM onset.

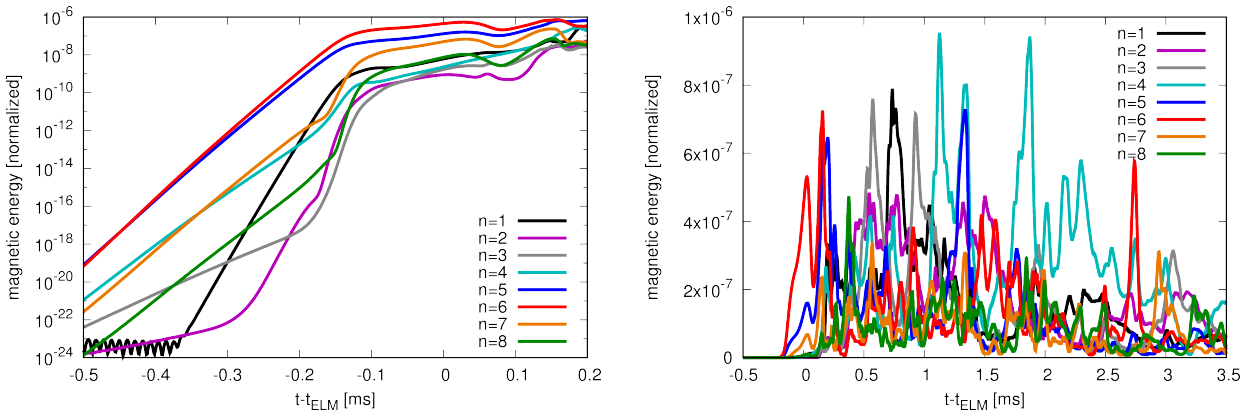

Figure 1: Evolution of magnetic energies for the individual harmonics versus time. Left: The logarithmic plot of the early ELM phase shows the drive of subdominant modes by linear mode coupling. Right: The non-logarithmic plot shows the that the perturbations are strongest at $t - t_{\mathrm{ELM}} = 0 \ldots 2\mathrm{ms}$ during which losses and divertor heat fluxes are high, while some activity remains after the crash and decays away relatively slowly.

3.3 Linear growth of the instability

In the ASDEX Upgrade ELM simulations, the linear instability growing out of a small non-axisymmetric initial perturbation is dominated by the $n = 6$ toroidal harmonic (see Fig. 1) with an eigenfunction localized to the outboard side of the plasma as it is typical for ballooning modes[1]. This is in line with the fact that the precursor modes observed prior to the ELM crash in these ASDEX Upgrade experiments are also localized to the outboard side of the plasma. The linear growth rate for the magnetic perturbation of $4 \pm 1 \cdot 10^4 s^{-1}$ agrees well with the experimental value of $5 \pm 2 \cdot 10^4 s^{-1}$ obtained by magnetic measurements, however the higher resistivity in the simulations as well as uncertainties in the equilibrium reconstruction can affect this comparison.

Neoclassical and diamagnetic flows [34] are crucial for reproducing experimental key observations. Without flows, far larger mode numbers become linearly dominant which is in line with infinite-n ballooning predictions and previous ASDEX Upgrade simulations which had not accounted for flow effects[28]. As a result, simulations without background flows lead to a spectrum during the crash very different from experimental observations. The ratio of energy lost to inner and outer divertor targets is only close to experimental observations when flows are included (see Section 3.6). Finally, these flows are necessary to reproduce experimental mode rotation[51].

3.4 Quadratic mode coupling

Quadratic mode coupling sets in significantly before the instability has reached a large enough amplitude to affect the background profiles and begins to saturate (compare also Ref.[37]). In the present case, for instance the $n = 5$ and $n = 6$ harmonics are driving the $n = 1$ mode as seen in the left part of Figure 1, which is linearly stable. The right part of the figure shows on a non-logarithmic scale the further evolution of energies across the ELM crash.

[1] The $n = 5$ growth rate is only slightly lower than the $n = 6$ growth rate.

There are various indications from experiments for the importance of quadratic mode coupling during ELM crashes. Strong low-n components were reported for instance in the TCV tokamak[82], which cannot be explained by linear stability analysis. Also magnetic structures observed during ELMs which are strongly localized to certain magnetic field lines and which consist of a large number of coherent modes[28, 83] are indicative for mode-coupling. Very recently, direct evidence of three-wave coupling during an ELM cycle was reported for ASDEX Upgrade in the discharge discussed here[78].

Refined evaluation methods for the magnetic measurements at ASDEX Upgrade[50] allow to extract the toroidal spectrum during an ELM cycle revealing dominant $n = 2 \ldots 5$ components[17] for the present discharge, corresponding to a clear shift from the linear stability analysis in which $n = 5, 6$ are dominating[2]. In the simulation, $n = 4$ is dominating during the ELM crash ($t - t_{\mathrm{ELM}} = 0 \ldots 2\mathrm{ms}$)[3] and $n = 1 \ldots 6$ have significant amplitudes, $n \geq 7$ are lower by at least a factor two in average energies. The $n = 1$ mode is important for the development of the non-linear spectrum during the ELM crash as demonstrated by the fact that identical simulations restricted to the $n = 0, 2, 4, 6, 8$ or $n = 0, 3, 6, 9$ harmonics lead to an ELM crash almost entirely dominated by $n = 6$.

In summary, growth rate as well as toroidal mode spectrum during the ELM crash are reproduced well in simulations if neoclassical and diamagnetic effects are included and the coupling to the $n = 1$ harmonic are taken into account. Recent experimental studies for ASDEX Upgrade suggest a strong dependency of the dominant toroidal mode number on q_{95}[16] (or respectively the plasma current) opening up promising opportunities for further comparisons.

3.5 Loss mechanisms

The ballooning modes leading to the ELM crash are associated with a strong kinetic as well as a magnetic perturbation of the plasma, which lead to two different loss mechanisms.

Convective losses The kinetic perturbation leads to the formation of ballooning fingers by an interchange-like $E \times B$ inward/outward motion of low/high pressure plasma in the very edge. The high pressure fingers in the scrape-off layer are partly sheared off by plasma flows induced during the crash by Maxwell stress leading to the formation of filaments elongated along the magnetic field lines as shown in Figure 2. Several such bursts are observed which is in line with experimental observations for long type-I ELMs[20]. The high-pressure structures expelled into the scrape off layer quickly lose energy towards the divertor by parallel heat conduction, the heat flux onto the main walls is typically low since the time scale for parallel conduction to the divertors is usually much shorter than the time scale

[2]Note, that the method applied cannot resolve $n = 1$ due to the large wave length and short time scales involved such that the $n = 1$ amplitude remains unknown in the experiment

[3]Note, that t_{ELM} is defined as the time where the heat flux in the outer divertor starts to rise significantly in order to be comparable to the experiment. The ELM crash is completed after about 2 ms, since losses and divertor heat fluxes drop significantly at that point.

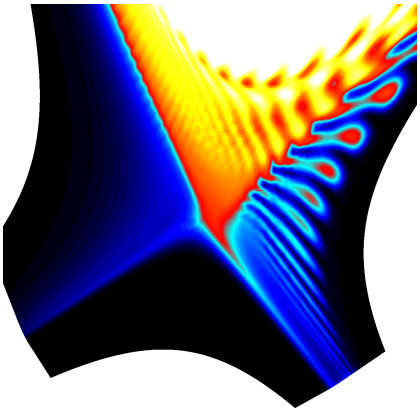

Figure 2: The pressure distribution around the X-point is shown during an ELM simulation. The formation of filaments can be observed, which quickly loose their pressure along magnetic field lines outside the separatrix. This simulation (taken from Ref. [29]) does not include background flows. When background flows are taken into account, ballooning fingers and filament formation are still observed in simulations, but the separation of the filaments from the main plasma becomes less pronounced.

for the filament convection to the wall. This is also the case in the present simulation, where the filaments have lost most of their energy before they come close to the wall.

Conductive losses The magnetic perturbations produced by the instabilities lead to the formation of islands. At larger amplitudes where these islands begin to overlap, flux surfaces are destroyed and a stochastic field region is formed [64]. As seen in Figure 3, the edge of the plasma becomes fully stochastic. The magnetic field lines in this region are directly connected to the divertor targets as the connection length plot of Figure 4 shows. However, from the $q = 3$ surface inwards, some of the KAM surfaces remain intact forming "magnetic barriers" [45, 63, 80, 85]. As a result, although stochastization is observed inside the q=3 surface, the connection length to the divertor targets remains infinite for this region. Figure 4 also shows experimental data for the propagation of the cold front produced by the ELM crash, which qualitatively agrees well with the evolution of the stochastic layer.

The region affected by convection due to the formation of ballooning fingers typically contains a larger fraction of the plasma particles than of the plasma thermal energy due to the very different density and temperature profiles. In the considered ASDEX Upgrade equilibrium, the region $\Psi_N = 0.95 \ldots 1$ contains about 6.6% of the particles and only 2.0% of the thermal energy. These numbers represent upper limits for the possible convective losses showing that convective losses. Conductive losses along the stochastic magnetic field lines mostly affect the electron temperature due to the large parallel electron heat conductivity.

In the present simulation, about 7% of the particles and 3% of the thermal energy are lost during the ELM crash, while the experiment sees values of $8 \pm 1\%$ of particle losses and $6 \pm 1\%$ of energy losses. Thus, the particle losses agree well, while the energy losses are underestimated in the simulation. This indicates that our choice of the parallel heat diffusion coefficient (reduced by two orders of magnitude compared to the Spitzer values in order to account

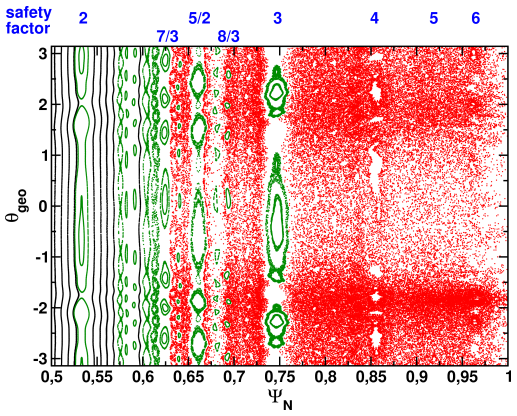

Figure 3: Poincaré plot of the magnetic structure at $t - t_{\mathrm{ELM}} = 1.21$ms. Stochastic regions are shown in red, islands in green, and normal closed flux surfaces in black. In the region outside the $q = 3$ surface, KAM surfaces have broken down such that a single stochastic region is formed. The stochastic regions inside $q = 3$ are separated by intact KAM surfaces as also seen in the connection length plot (Fig.4).

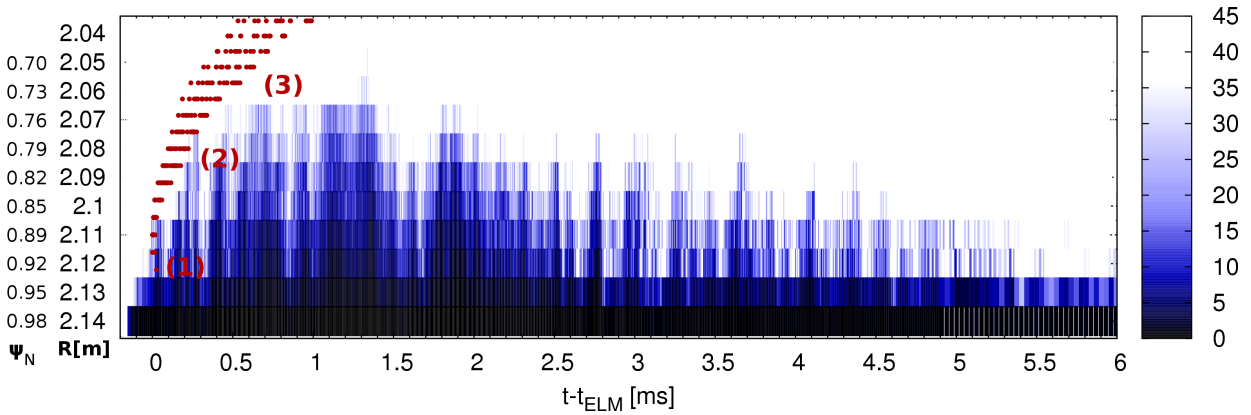

Figure 4: The connection length (in km) at various radial locations from the midplane to the divertor targets along magnetic field lines is plotted over time (white: no connection to the divertor). Stochasticity appears with a very fast first burst at $t - t_{\mathrm{ELM}} = 0$ms and successively grows further inwards within $\approx 300\mu$s. Both in time scales and radial region, the stochastic layer formation agrees well with the cold front propagation measured in experiments (red dots, see Reference [75] for a detailed analysis) obtained for similar plasma configurations (same plasma current): In the very edge, almost instantaneous propagation probably due to the first stochastic burst and convective losses (1), then propagation on a fast time scale following roughly the growth of the edge stochastic layer connected to the divertor targets (2), and further inwards slower propagation supposedly dominated by islands and local stochastic field regions (3). After the main ELM crash ($t - t_{\mathrm{ELM}} > 2$ms), the stochastic region disappears slowly.

for the heat flux limit) is not appropriate. A proper treatment of the heat flux limit will be implemented for future simulations. The ELM duration defined by the time during which significant losses and divertor heat fluxes are observed is about 2 ms both in the experiment and simulations corresponding to so called long ELMs [19, 20].

3.6 Divertor heat loads

In ASDEX Upgrade and other devices[11, 12], total heat fluxes towards inner and outer divertor are comparable in normal magnetic field orientation. In the present ASDEX Upgrade simulations, about 40% of the energy are transported towards the inner and 60% towards the outer divertorcomparable to experimental observations. In simulations without neoclassical and diamagnetic flows, a much stronger heat flux towards the outer divertor is observed[58]. Since the experiment observes a pronounced heatflux towards the outer divertor in reversed field operation[11, 12], additional comparisons will be performed to verify whether this trend is reproduced.

The peak heat fluences in JET ELM simulations were compared for a large number of equilibria[59, 60] to the experimentally observed scaling[13]. Simulations without background flows show excellent agreement regarding energy losses and peak heat fluences, however do not reproduce the distribution of heat between inner and outer divertor legs of experiments. Simulations including background flows reproduce well the distribution between inner and outer divertor legs, but underestimate ELM energy losses and peak heat fluences. Thus, in spite of very encouraging agreement in this respect, remaining inconsistencies are under investigation.

3.7 Decay of the MHD activity

The drop of edge pressure gradient and current density in the pedestal region during the ELM crash acts stabilizing onto the linear instability. On the other hand, the stabilizing $E \times B$ and diamagnetic flows are reduced as well since they are following the pressure gradient evolution. Also, the ELM crash is associated with strongly localized structures such that even when the flux surface averaged pressure profiles are flattened considerably, large local gradients may be present. Similar to the recently observed ballooning modes localized to certain field lines with applied RMP fields[84], this can give rise to local instabilities. As a result, the instability does not decay away as fast as it would be expected from the simplified linear pictures. The mechanism for the formation of short and long ELMs often even in the same discharge is under investigation in the experiment (see e.g. Reference[20, 66]) and will also be studied in future simulations. The interplay of stabilizing and destabilizing effects is also crucial for the formation of cyclic ELM crashes. Based on first demonstrations of multi ELM cycle simulations[2, 55] with repetition frequencies significantly higher than for type-I ELMs, we will continue our efforts to reproduce full type-I ELM cycles.

3.8 Tungsten transport

In order to obtain a good performance of ITER, the impurity concentration in the plasma needs to be kept below certain thresholds. Tungsten is a particularly important impurity since it is used as divertor material and is not completely ionized even at temperatures of several keV leading to strong radiative losses. ELMs can control the

tungsten concentration in the plasma by expelling tungsten particles. The full orbit particle tracer of JOREK [76, 77], which accounts for the evolution of ionization states and collisions with the background plasma, allows to study this.

Based on the ASDEX Upgrade ELM simulations discussed in the previous sections, Tungsten transport is investigated[4]. Several million test particles are initialized covering the whole relevant area ranging from the outer core plasma to the scrape off layer. During the ELM crash, a strong radial mixing is observed. The radial motion of the particles is caused by the perturbation of the electric field during the crash. Within 1 ms of the ELM crash, about 10% of the particles from the pedestal region ($\Psi_N = 0.95 \dots 1$) are lost across the separatrix, while about 15% of the particles from the scrape off layer ($\Psi_N = 1 \dots 1.05$) are transferred into the plasma. Since the tungsten particle density inside the separatrix is much larger than in the SOL before the ELM crash[10], a significant net exhaust of tungsten particles is observed. A detailed analysis will be presented in Reference [77].

4 ELM control

The strong localized heat loads onto divertor targets expected in ITER give rise to research on various approaches for ELM control. At the same time, a sufficient ELM frequency (or substitution by different mechanisms) is important to keep the impurity concentration in the plasma at a tolerable level. This section gives a brief overview of the most relevant approaches for ELM control. The basic principles are explained and referring to related simulations.

Quiescent H-Mode Natural ELM free regimes like the Quiescent H-Mode (QH-Mode)[5, 23] have been found in various tokamak experiments and are an important subject of present research. QH-Mode is characterized by a pedestal comparable to H-Mode plasmas, the absence of ELM crashes, and a saturated rotating mode in the pedestal region causing a characteristic perturbation of density and temperature (edge harmonic oscillation, EHO). QH-Mode seems to be obtained best with strong plasma shaping, large edge current densities (i.e., low collisionalities), strong edge flow shears, and in reversed field operation. Key aspects of QH-Mode like saturated modes in the pedestal region with low toroidal mode numbers, and the resulting EHO have been reproduced sucessfully in JOREK simulations[42, 43], identifying the EHO as a saturated kink-peeling mode. These modes induce an enhanced particle transport across the pedestal region, which is beneficial for limiting the impurity accumulation in the plasma. Nonlinear mode coupling leads to the toroidal localization of the EHO. The mechanisms determining whether a certain plasma configuration enters an ELMing H-Mode or QH-Mode are under investigation.

Pellet ELM triggering The injection of pellets to trigger ELMs more frequently than they would occur naturally[41] has proven successful in many experiments and allows to reduce ELM energy losses[39]. Whether the

[4] Background collisions have not been accounted since the collision time of tungsten ions with the background plasma assuming a 1% Beryllium concentration is longer than the time scale of MHD fluctuations.

peak heat fluxes can also be mitigated with this method is not definitely answered. The mechanism of pellet ELM triggering[21, 33, 40, 72] has been identified by JOREK simulations of pellet injection: When the pellet ablates adiabatically, the pressure in the pellet cloud remains unchanged while the electron density is strongly increasing and the temperature strongly decreasing. Due to the fast heat transport along magnetic field lines, the pellet cloud is reheated faster than the density decreases by parallel convection. Thus, a strong 3D perturbation of the pressure forms, driving the plasma locally beyond the ballooning stability threshold such that an ELM crash sets in. Simulations for DIII-D have demonstrated a clear threshold in the pellet size for destabilizing ELMs which agrees reasonably well with the experimental observations[21]. Validation against other devices as well as predictive simulations for ITER are ongoing. Additionally, simulations are presently refined by the inclusion of background flows.

Vertical kick ELM triggering The destabilization of ELMs by magnetic kicks was demonstrated in several tokamak devices[7, 39]. Although, a destabilization by an increase of the edge current density was suspected, the exact mechanisms remained unclear. Recent simulations with the free boundary JOREK-STARWALL[28] for a realistic ITER 7.5MA/2.65T plasma have now shown that ELMs are indeed destabilized by an increase of the edge current density[1]. The mechanisms changing the current density have been revealed to be strongly related to plasma compression, allowing to optimize the coil current time traces for kicks. In line with experimental observations, the destabilization always appears at the same vertical axis position independent of the kick velocity for a given equilibrium. Additionally, a plasma which is already peeling-ballooning unstable can be driven back into the stable regime by a kick in the opposite direction explaining that with the sinosoidal kicks performed in experiments, ELMs always occur in the same phase during which the plasma is compressed by the kick. After additional validation against existing experiments, it will be investigated how peak heat fluxes of the triggered ELMs compare with natural ELMs.

Mitigation or suppression by RMP fields Mitigation and suppression of ELMs by the application of resonant magnetic perturbation coils (RMPs) has been observed in various experiments[14, 74]. Early JOREK simulations of the penetration of RMP fields into the plasma[52] have been refined by the inclusion of two-fluid effects[3, 57] reproducing well the 3D displacement of the flux surfaces observed in the experiments. The mitigation and suppression of ELMs is presently thought to be caused by either edge stochastization or the presence of a magnetic island at the pedestal top, reducing the pressure gradient in the pedestal below the peeling-ballooning threshold. However, JOREK simulations[3, 56] indicate, that non-linear mode coupling could play an important role as well. In Reference [56], it is shown for ASDEX Upgrade geometry, that RMP fields can hinder ballooning modes from growing exponentially. This is observed only in the so-called resonant configuration of RMP coil currents consistent with ELM suppression in ASDEX Upgrade experiments. The exact mechanisms are under investigation.

5 Conclusions

An overview over the JOREK code and its recent applications to ELM physics has been given. Many key features of type-I ELMs and of ELM control methods from the experiments are reproduced very well in the simulations such that predictive simulations become more and more feasible.

A type-I ELM crash in ASDEX Upgrade was compared in detail to experimental observations. The linear instability has ballooning character as it is also seen for modes just before the ELM onset in the experiment, and linear growth rates agree well. Due to quadratic mode coupling, the $n = 4$ mode is dominating during the ELM crash comparable to the dominant $n = 3$ in the experiment. Also, neoclassical and diamagnetic flows are crucial for obtaining a mode spectrum comparable to the experiment. Recent experimental observations directly prove the mode coupling during an ELM cycle. The ELM crash takes about 2 ms both in the experiment as well as in the simulations ("long ELM"). The convective losses due to the formation of ballooning fingers and the conductive losses due to the formation of a stochastic layer in the plasma edge were discussed in detail. The evolution of the stochastic layer agrees well with the experimentally observed propagation of the ELM cold front. Total particle losses during the ELM agree very well between experiment and simulations, while losses of the thermal energy are underestimated in the simulations. Most likely, this is due to an underestimation of conductive losses by the applied parallel heat diffusivity. The ELM heat load is almost evenly distributed between inner (40%) and outer (60%) divertor target in line with experimental observations for normal field operation. Without the inclusion of neoclassical and diamagnetic flows, almost the entire heat load goes to the outer divertor target. Tungsten transport by the ELM crash is under investigation and shows already good qualitative agreement with the experiment, quantitative comparisons are ongoing. Published results for JET show a good agreement of peak heat fluences with experimental scaling. However, when background flows are included, heat fluences are underestimated, which needs further investigations.

Regarding ELM control, a brief overview of JOREK activities in the fields of QH-Mode, pellet ELM triggering, magnetic kick ELM triggering, and ELM mitigation/suppression by RMP fields was given.

Future activities will concentrate on improving the models to further improve the agreement with the experiment. This will include for instance pushing simulations to fully realistic resistivity values, improving the scrape off layer model. Additional validation will be done based on observations from various devices both for ELM crashes as well as for the control methods under investigation. Based on this, predictions for ITER will be possible more and more accurately. Obtaining fully realistic type-I ELM cycles is an important goal, allowing to study also the inter-ELM phase and the ELM onset in detail. Understanding the differences between short and long ELMs and small ELM regimes will be important research topics as well.

Acknowledgments

This work has been carried out within the framework of the EUROfusion Consortium and has received funding from the Euratom research and training programme 2014-2018 under grant agreement No 633053. The views and opinions expressed herein do not necessarily reflect those of the European Commission.

References

[1] F. J. Artola, G. T. A. Huysmans, M Hoelzl, P Beyer, A Loarte, Y Gribov, *Nuclear Fusion*, in preparation.

[2] M. Bécoulet, M. Kim, G. Yun, S. Pamela, J. Morales, X. Garbet, G. T. A. Huijsmans, C. Passeron, O. Fevrier, M. Hoelzl, A. Lessig, F. Orain, *Nuclear Fusion* **2017**, *57*(*11*), 116059.

[3] M. Bécoulet, F. Orain, G. T. A. Huijsmans, S. Pamela, P. Cahyna, M. Hoelzl, X. Garbet, E. Franck, E. Sonnendrücker, G. Dif-Pradalier, C. Passeron, G. Latu, J. Morales, E. Nardon, A. Fil, B. Nkonga, A. Ratnani, V. Grandgirard, *Phys. Rev. Lett.* **2014Sep**, *113*, 115001.

[4] A Burckhart, E Wolfrum, R Fischer, K Lackner, H Zohm, the ASDEX Upgrade Team, *Plasma Physics and Controlled Fusion* **2010**, *52*(*10*), 105010.

[5] K H Burrell, M E Austin, D P Brennan, J C DeBoo, E J Doyle, P Gohil, C M Greenfield, R J Groebner, L L Lao, T C Luce, M A Makowski, G R McKee, R A Moyer, T H Osborne, M Porkolab, T L Rhodes, J C Rost, M J Schaffer, B W Stallard, E J Strait, M R Wade, G Wang, J G Watkins, W P West, L Zeng, *Plasma Physics and Controlled Fusion* **2002**, *44*(*5A*), A253.

[6] O. Czarny, G. Huysmans, *Journal of Computational Physics* **2008**, *227*(*16*), 7423 –7445.

[7] A W Degeling, Y R Martin, J B Lister, L Villard, V N Dokouka, V E Lukash, R R Khayrutdinov, *Plasma Physics and Controlled Fusion* **2003**, *45*(*9*), 1637.

[8] A. Diallo, J. W. Hughes, M. Greenwald, B. LaBombard, E. Davis, S-G. Baek, C. Theiler, P. Snyder, J. Canik, J. Walk, T. Golfinopoulos, J. Terry, M. Churchill, A. Hubbard, M. Porkolab, L. Delgado-Aparicio, M. L. Reinke, A. White, A. C-M. team, *Phys. Rev. Lett.* **2014Mar**, *112*, 115001.

[9] E. J. Doyle, R. J. Groebner, K. H. Burrell, P. Gohil, T. Lehecka, N. C. L. Jr., H. Matsumoto, T. H. Osborne, W. A. Peebles, R. Philipona, *Physics of Fluids B: Plasma Physics* **1991**, *3*(*8*), 2300–2307, available at http://dx.doi.org/10.1063/1.859597.

[10] R. Dux, A. Janzer, T. Puetterich, ASDEX Upgrade Team, *Nuclear Fusion* **2011**, *51*(*5*), 053002.

[11] T Eich, A Herrmann, J Neuhauser, R Dux, J C Fuchs, S GÃijnter, L D Horton, A Kallenbach, P T Lang, C F Maggi, M Maraschek, V Rohde, W Schneider, the ASDEX Upgrade Team, *Plasma Physics and Controlled Fusion* **2005**, *47*(*6*), 815.

[12] T. Eich, A. Kallenbach, W. Fundamenski, A. Herrmann, V. Naulin, *Journal of Nuclear Materials* **2009**, *390*(*Supplement C*), 760 –763. Proceedings of the 18th International Conference on Plasma-Surface Interactions in Controlled Fusion Device.

[13] T. Eich, B. Sieglin, A. J. Thornton, M. Faitsch, A. Kirk, A. Herrmann, W. Suttrop, *Nuclear Materials and Energy* **2017**, *12*, 84.

[14] T. E. Evans, M. E. Fenstermacher, R. A. Moyer, T. H. Osborne, J. G. Watkins, P. Gohil, I. Joseph, M. J. Schaffer, L. R. Baylor, M. BÃĪcoulet, J. A. Boedo, K. H. Burrell, J. S. deGrassie, K. H. Finken, T. Jernigan, M. W. Jakubowski, C. J. Lasnier, M. Lehnen, A. W. Leonard, J. Lonnroth, E. Nardon, V. Parail, O. Schmitz, B. Unterberg, W. P. West, *Nuclear Fusion* **2008**, *48*(*2*), 024002.

[15] A. Fil, E. Nardon, M. Hoelzl, G. T. A Huijsmans, F. Orain, M. Becoulet, P. Beyer, G. Dif-Pradalier, R. Guirlet, H. R. Koslowski, M. Lehnen, J. Morales, S. Pamela, C. Passeron, C. Reux, F. Saint-Laurent, *Physics of Plasmas* **2015**, *22*(*6*), 062509, available at http://dx.doi.org/10.1063/1.4922846.

[16] F.Mink, et al, *private communication* **2017**.

[17] F.Mink, M.Hoelzl, E.Wolfrum, F.Orain, M.Dunne, A.Lessig, S.Pamela, P.Manz, M.Maraschek, G.T.A.Huijsmans, M.Becoulet, F.M.Laggner, M.Cavedon, K.Lackner, S.Günter, U.Stroth, the ASDEX Upgrade Team, *Nuclear Fusion* **2018**, *58*, 026011.

[18] Franck, Emmanuel, Hoelzl, Matthias, Lessig, Alexander, Sonnendrücker, Eric, *ESAIM: M2AN* **2015**, *49*(*5*), 1331–1365.

[19] L. Frassinetti, D. Dodt, M. N. A. Beurskens, A. Sirinelli, J. E. Boom, T. Eich, J. Flanagan, C. Giroud, M. S. Jachmich, M. Kempenaars, P. Lomas, G. Maddison, C. Maggi, R. Neu, I. Nunes, C. P. von Thun, B. Sieglin, M. Stamp, J.-E. Contributors, *Nuclear Fusion* **2015**, *55*(*2*), 023007.

[20] L. Frassinetti, M. G. Dunne, M. Beurskens, E. Wolfrum, A. Bogomolov, D. Carralero, M. Cavedon, R. Fischer, F. M. Laggner, R. M. McDermott, H. Meyer, G. Tardini, E. Viezzer, the EUROfusion MST1 Team, the ASDEX-Upgrade Team, *Nuclear Fusion* **2017**, *57(2)*, 022004.

[21] S. Futatani, G. Huijsmans, A. Loarte, L. R. Baylor, N. Commaux, T. C. Jernigan, M. E. Fenstermacher, C. Lasnier, T. H. Osborne, B. PegouriÃľ, *Nuclear Fusion* **2014**, *54(7)*, 073008.

[22] P. Gohil, M. Ali Mahdavi, L. Lao, K. H. Burrell, M. S. Chu, J. C. DeBoo, C. L. Hsieh, N. Ohyabu, R. T. Snider, R. D. Stambaugh, R. E. Stockdale, *Phys. Rev. Lett.* **1988Oct**, *61*, 1603–1606.

[23] C. M. Greenfield, K. H. Burrell, J. C. DeBoo, E. J. Doyle, B. W. Stallard, E. J. Synakowski, C. Fenzi, P. Gohil, R. J. Groebner, L. L. Lao, M. A. Makowski, G. R. McKee, R. A. Moyer, C. L. Rettig, T. L. Rhodes, R. I. Pinsker, G. M. Staebler, W. P. West, the DIII-D Team, *Phys. Rev. Lett.* **2001May**, *86*, 4544–4547.

[24] J. W. Haverkort, H. J. de Blank, G. T. A. Huysmans, J. Pratt, B. Koren, *Journal of Computational Physics* **2016**, *316*, 281 –302.

[25] P. Hénon, P. Ramet, J. Roman, *Parallel Computing* **2002**, *28(2)*, 301 –321.

[26] M. Hoelzl, S. Guenter, I. G. J. Classen, Q. Yu, the TEXTOR Team, E. Delabie, *Nuclear Fusion* **2009**, *49(11)*, 115009.

[27] M. Hoelzl, S. Guenter, R. P. Wenninger, W.-C. Mueller, G. T. A. Huysmans, K. Lackner, I. Krebs, *Physics of Plasmas* **2012**, *19(8)*, 082505, available at http://dx.doi.org/10.1063/1.4742994.

[28] M. Hoelzl, S. Guenter, R. P. Wenninger, W.-C. Mueller, G. T. A. Huysmans, K. Lackner, I. Krebs, *Physics of Plasmas* **2012**, *19(8)*, 082505, available at http://dx.doi.org/10.1063/1.4742994.

[29] M. Hoelzl, S. Günter, ASDEX Upgrade Team. (). *Reduced MHD simulations of edge localized modes in ASDEX Upgrade*, 38th European Physical Society Conference on Plasma Physics (EPS), Strasbourg, France, pp. P2.078.

[30] M Hoelzl, G T A Huijsmans, P Merkel, C Atanasiu, K Lackner, E Nardon, K Aleynikova, F Liu, E Strumberger, R McAdams, I Chapman, A Fil, *Journal of Physics: Conference Series* **2014**, *561(1)*, 012011.

[31] D. Hu, E. Nardon, G. T. A. Huijsmans, M. Lehnen. (). *Investigation of MHD activity caused by shattered pellet injection via JOREK 3D non-linear MHD simulation*, 44th European Physical Society Conference on Plasma Physics (EPS), Belfast, Northern Ireland, pp. P2.142.

[32] G. T. A. Huijsmans, C. S. Chang, N. Ferraro, L. Sugiyama, F. Waelbroeck, X. Q. Xu, A. Loarte, S. Futatani, *Physics of Plasmas* **2015**, *22(2)*, 021805, available at http://dx.doi.org/10.1063/1.4905231.

[33] G T A Huysmans, S Pamela, E van der Plas, P Ramet, *Plasma Physics and Controlled Fusion* **2009**, *51(12)*, 124012.

[34] G. T. A. Huysmans, S. E. Sharapov, A. B. Mikhailovskii, W. Kerner, *Physics of Plasmas* **2001**, *8(10)*, 4292–4305, available at http://dx.doi.org/10.1063/1.1398573.

[35] G. T. A. Huysmans, O. Czarny, *Nuclear Fusion* **2007**, *47(7)*, 659.

[36] M Keilhacker, G Becker, K Bernhardi, A Eberhagen, M ElShaer, G FuBmann, O Gehre, J Gernhardt, G v Gierke, E Glock, G Haas, F Karger, S Kissel, O Kluber, K Kornherr, K Lackner, G Lisitano, G G Lister, J Massig, H M Mayer, K McCormick, D Meisel, E Meservey, E R Muller, H Murmann, H Niedermeyer, W Poschenrieder, H Rapp, B Richter, H Rohr, F Ryter, F Schneider, S Siller, P Smeulders, F Soldner, E Speth, A Stabler, K Steinmetz, K-H Steuer, Z Szymanski, G Venus, O Vollmer, F Wagner, *Plasma Physics and Controlled Fusion* **1984**, *26(1A)*, 49.

[37] I. Krebs, M. Hoelzl, K. Lackner, S. Guenter, *Physics of Plasmas* **2013**, *20(8)*, 082506, available at http://dx.doi.org/10.1063/1.4817953.

[38] F M Laggner, E Wolfrum, M Cavedon, F Mink, E Viezzer, M G Dunne, P Manz, H Doerk, G Birkenmeier, R Fischer, S Fietz, M Maraschek, M Willensdorfer, F Aumayr, the EUROfusion MST1 Team, the ASDEX Upgrade Team, *Plasma Physics and Controlled Fusion* **2016**, *58(6)*, 065005.

[39] P T Lang, A W Degeling, J B Lister, Y R Martin, P J M. Carthy, A C C Sips, W Suttrop, G D Conway, L Fattorini, O Gruber, L D Horton, A Herrmann, M E Manso, M Maraschek, V Mertens, A MÃijck, W Schneider, C Sihler, W Treutterer, H Zohm, ASDEX Upgrade Team, *Plasma Physics and Controlled Fusion* **2004**, *46(11)*, L31.

[40] P. T. Lang, K. Lackner, M. Maraschek, B. Alper, E. Belonohy, K. GÃąl, J. Hobirk, A. Kallenbach, S. KÃąlvin, G. Kocsis, C. P. P. von Thun, W. Suttrop, T. Szepesi, R. Wenninger, H. Zohm, the ASDEX Upgrade Team, JET-EFDA contributors, *Nuclear Fusion* **2008**, *48(9)*, 095007.

[41] P. T. Lang, H. Zohm, K. Buchl, J. C. Fuchs, O. Gehre, O. Gruber, V. Mertens, H. W. Muller, J. Neuhauser, *Nuclear Fusion* **1996**, *36(11)*, 1531.

[42] F. Liu, G. T. A. Huijsmans, A. Loarte, A. M. Garofalo, W. M. Solomon, M. Hoelzl, B. Nkonga, S. Pamela, M. Becoulet, F. Orain, D. Van Vugt, *Plamas Physics and Controlled Fusion* **2018**, *60*, 014039.

[43] F. Liu, G. T. A. Huijsmans, A. Loarte, A. M. Garofalo, W. M. Solomon, P. B. Snyder, M. Hoelzl, L. Zeng, *Nuclear Fusion* **2015**, *55*(*11*), 113002.

[44] A Loarte, G Saibene, R Sartori, D Campbell, M Becoulet, L Horton, T Eich, A Herrmann, G Matthews, N Asakura, A Chankin, A Leonard, G Porter, G Federici, G Janeschitz, M Shimada, M Sugihara, *Plasma Physics and Controlled Fusion* **2003**, *45*(*9*), 1549.

[45] R. S. MacKay, *Physica D: Nonlinear Phenomena* **1983**, *7*(*1*), 283 –300.

[46] R. C. Malone, R. L. McCrory, R. L. Morse, *Phys. Rev. Lett.* **1975Mar**, *34*, 721–724.

[47] P. J McCarthy, P. Martin, W. Schneider, The CLISTE interpretive equilibrium code **1999**.

[48] P. Merkel, E. Strumberger, *ArXiV* **2015**, 1508.04911.

[49] D. Meshcheriakov, V. Igochine, S. Fietz, M. Hoelzl, F. Orain, S. Günter, H. Zohm. *Tearing mode seeding by externally provided resonant magnetic perturbations*, 44th European Physical Society Conference on Plasma Physics (EPS), Belfast, Northern Ireland.

[50] F. Mink, E. Wolfrum, M. Maraschek, H. Zohm, L. Horvath, F. M Laggner, P. Manz, E. Viezzer, U. Stroth, the ASDEX Upgrade Team, *Plasma Physics and Controlled Fusion* **2016**, *58*(*12*), 125013.

[51] J. A. Morales, M. BÃľcoulet, X. Garbet, F. Orain, G. Dif-Pradalier, M. Hoelzl, S. Pamela, G. T. A. Huijsmans, P. Cahyna, A. Fil, E. Nardon, C. Passeron, G. Latu, *Physics of Plasmas* **2016**, *23*(*4*), 042513, available at http://dx.doi.org/10.1063/1.4947201.

[52] E. Nardon, M. Bécoulet, G. Huysmans, O. Czarny, *Physics of Plasmas* **2007**, *14*(*9*), 092501, available at http://dx.doi.org/10.1063/1.2759889.

[53] E Nardon, A Fil, M Hoelzl, G Huijsmans, J. contributors, *Plasma Physics and Controlled Fusion* **2017**, *59*(*1*), 014006.

[54] F. Orain, M. Bécoulet, G. Dif-Pradalier, G. Huijsmans, S. Pamela, E. Nardon, C. Passeron, G. Latu, V. Grandgirard, A. Fil, A. Ratnani, I. Chapman, A. Kirk, A. Thornton, M. Hoelzl, P. Cahyna, *Physics of Plasmas* **2013**, *20*(*10*), 102510, available at http://dx.doi.org/10.1063/1.4824820.

[55] F. Orain, M. Bécoulet, G. T. A. Huijsmans, G. Dif-Pradalier, M. Hoelzl, J. Morales, X. Garbet, E. Nardon, S. Pamela, C. Passeron, G. Latu, A. Fil, P. Cahyna, *Phys. Rev. Lett.* **2015Jan**, *114*, 035001.

[56] F. Orain, M. Hoelzl, et al, *Physics of Plasmas* **in preparation**.

[57] F. Orain, M. Hoelzl, E. Viezzer, M. Dunne, M. Becoulet, P. Cahyna, G. T. A. Huijsmans, J. Morales, M. Willensdorfer, W. Suttrop, A. Kirk, S. Pamela, S. Guenter, K. Lackner, E. Strumberger, A. Lessig, the ASDEX Upgrade Team, the EUROfusion MST1 Team, *Nuclear Fusion* **2017**, *57*(*2*), 022013.

[58] F. Orain, M Becoulet, J Morales, G T A Huijsmans, G Dif-Pradalier, M Hoelzl, X Garbet, S Pamela, E Nardon, C Passeron, G Latu, A Fil, P Cahyna, *Plasma Physics and Controlled Fusion* **2015**, *57*(*1*), 014020.

[59] S Pamela, T Eich, L Frassinetti, B Sieglin, S Saarelma, G Huijsmans, M Hoelzl, M Becoulet, F Orain, S Devaux, I Chapman, I Lupelli, E Solano, J. Contributors, *Plasma Physics and Controlled Fusion* **2016**, *58*(*1*), 014026.

[60] S. J. P. Pamela, G. T. A. Huijsmans, T. Eich, S. Saarelma, I. Lupelli, C. F. Maggi, C. Giroud, I. T. Chapman, S. F. Smith, L. Frassinetti, M. Becoulet, M. Hoelzl, F. Orain, S. Futatani, J. Contributors, *Nuclear Fusion* **2017**, *57*(*7*), 076006.

[61] C. P. Perez, H. R. Koslowski, G. T. A. Huysmans, T. C. Hender, P. Smeulders, B. Alper, E. de la Luna, R. J. Hastie, L. Meneses, M. F. F. Nave, V. Parail, M. Zerbini, J.-E. Contributors, *Nuclear Fusion* **2004**, *44*(*5*), 609.

[62] J. Pratt, G. T. A. Huijsmans, E. Westerhof, *Physics of Plasmas* **2016**, *23*(*10*), 102507, available at http://dx.doi.org/10.1063/1.4964785.

[63] A. B. Rechester, T. H. Stix, *Phys. Rev. A* **1979Apr**, *19*, 1656–1665.

[64] M. N. Rosenbluth, R. Z. Sagdeev, J. B. Taylor, G. M. Zaslavski, *Nuclear Fusion* **1966**, *6*(*4*), 297.

[65] O. Sauter, C. Angioni, Y. R. Lin-Liu, *Physics of Plasmas* **1999**, *6*(*7*), 2834–2839, available at http://dx.doi.org/10.1063/1.873240.

[66] P A Schneider, E Wolfrum, M G. Dunne, R Dux, A Gude, B Kurzan, T Puetterich, S K. Rathgeber, J Vicente, A Weller, R Wenninger, the ASDEX Upgrade Team, *Plasma Physics and Controlled Fusion* **2014**, *56*(*2*), 025011.

[67] B Sieglin, T Eich, A Scarabosio, G Arnoux, I Balboa, S Devaux, A Herrmann, F Hoppe, M Hoelzl, A Kallenbach, P Lang, G F Matthews, S Marsen, S Pamela, M Rack, R Wenninger, the ASDEX Upgrade Team, JET EFDA Contributors, *Plasma Physics and Controlled Fusion* **2013**, *55*(*12*), 124039.

[68] P. B. Snyder, T. H. Osborne, K. H. Burrell, R. J. Groebner, A. W. Leonard, R. Nazikian, D. M. Orlov, O. Schmitz, M. R. Wade, H. R. Wilson, *Physics of Plasmas* **2012**, *19*(*5*), 056115, available at http://dx.doi.org/10.1063/1.3699623.

[69] P. B. Snyder, H. R. Wilson, J. R. Ferron, L. L. Lao, A. W. Leonard, D. Mossessian, M. Murakami, T. H. Osborne, A. D. Turnbull, X. Q. Xu, *Nuclear Fusion* **2004**, *44(2)*, 320.

[70] C. Sommariva, E. Nardon, P. Beyer, M. Hoelzl, G. T. A. Huysmans, D. van Vugt, JET Contributors, *Nuclear Fusion* **2018**, *58*, 016043.

[71] L. Spitzer, R. Härm, *Phys. Rev.* **1953Mar**, *89*, 977–981.

[72] H. R. Strauss, W. Park, *Physics of Plasmas* **1998**, *5(7)*, 2676–2686, available at http://dx.doi.org/10.1063/1.872955.

[73] U. Stroth, et al, *Nuclear Fusion* **2013**, *53(10)*, 104003.

[74] W. A. Suttrop, R. Nazikian, A. Kirk, V. Bobkov, M. Cavedon, M. Dunne, T E.Evans, B A.Grierson, A W.Hyatt, Y Q.Liu, B Lyons, R M.McDermott, H Meyer, T Odstrcil, D Orlov, T H.Osborne, C Paz-Soldan, D A.Ryan, E Viezzer, M Willensdorfer, ASDEX Upgrade Team, MST1 team, DIII-D team, *Physical Review Letters* **submitted**.

[75] E. Trier, E. Wolfrum, M. Willensdorfer, Q. Yu, F. Ryter, C. Angioni, F. Orain, M. Hoelzl, M. G. Dunne, S. Denk, J. C. Fuchs, R. Fischer, P. Hennequin, B. Kurzan, F. Mink, A. Mlynek, T. Odstrcil, P. A. Schneider, U. Stroth, B. Vanovac, the ASDEX Upgrade Team, the EUROfusion MST1 Team, *Nuclear Fusion*, submitted.

[76] D. C. van Vugt, G. T. A. Huijsmans, M. Hoelzl, L. P. J. Kamp, N. J. Lopes Cardoso, A. Loarte. *Kinetic simulations of w impurity transport by ELMs*, 44th European Physical Society Conference on Plasma Physics (EPS), Belfast, Northern Ireland.

[77] D. C. van Vugt, G. T. A. Huijsmans, M. Hoelzl, L. P. J. Kamp, N. J. Lopes Cardozo, A Loarte, *Plasma Physics and Controlled Fusion*, in preparation.

[78] B. Vanovac, E. Wolfrum, et al., *Nuclear Fusion* **submitted**.

[79] E. Viezzer, T. Puetterich, C. Angioni, A. Bergmann, R. Dux, E. Fable, R. M. McDermott, U. Stroth, E. Wolfrum, the ASDEX Upgrade Team, *Nuclear Fusion* **2014**, *54(1)*, 012003.

[80] F. A. Volpe, J. Kessler, H. Ali, T. E. Evans, A. Punjabi, *Nuclear Fusion* **2012**, *52(5)*, 054017.

[81] F. Wagner, G. Becker, K. Behringer, D. Campbell, A. Eberhagen, W. Engelhardt, G. Fussmann, O. Gehre, J. Gernhardt, G. v. Gierke, G. Haas, M. Huang, F. Karger, M. Keilhacker, O. Klüber, M. Kornherr, K. Lackner, G. Lisitano, G. G. Lister, H. M. Mayer, D. Meisel, E. R. Müller, H. Murmann, H. Niedermeyer, W. Poschenrieder, H. Rapp, H. Röhr, F. Schneider, G. Siller, E. Speth, A. Stäbler, K. H. Steuer, G. Venus, O. Vollmer, Z. Yü, *Phys. Rev. Lett.* **1982**, *49*, 1408–1412.

[82] R. P. Wenninger, H. Reimerdes, O. Sauter, H. Zohm, *Nuclear Fusion* **2013**, *53(11)*, 113004.

[83] R. P. Wenninger, H. Zohm, J. E. Boom, A. Burckhart, M. G. Dunne, R. Dux, T. Eich, R. Fischer, C. Fuchs, M. Garcia-Munoz, V. Igochine, M. Hoelzl, L. N. C. Jr, T. Lunt, M. Maraschek, H. W. MÃijller, H. K. Park, P. A. Schneider, F. Sommer, W. Suttrop, E. Viezzer, the ASDEX Upgrade Team, *Nuclear Fusion* **2012**, *52(11)*, 114025.

[84] M. Willensdorfer, T. B. Cote, C. C. Hegna, W. Suttrop, H. Zohm, M. Dunne, E. Strumberger, G. Birkenmeier, S. S. Denk, F. Mink, B. Vanovac, L. C. Luhmann, *Phys. Rev. Lett.* **2017Aug**, *119*, 085002.

[85] H. Wobig, *Zeitschrift für Naturforschung A* **1987**, *42*, 1054–1066.

[86] E Wolfrum, A Burckhart, R Fischer, N Hicks, C Konz, B Kurzan, B Langer, T PÃijtterich, H Zohm, the ASDEX Upgrade Team, *Plasma Physics and Controlled Fusion* **2009**, *51(12)*, 124057.

[87] H Zohm, *Plasma Physics and Controlled Fusion* **1996**, *38(2)*, 105.